J Eng Math (2011) 71:185–203
DOI 10.1007/s10665-010-9445-1

Numerical study of the effect of nonlinear control on the behavior of a liquid drop in elongational flow with vorticity

Marco A. H. Reyes · A. A. Minzoni · E. Geffroy

Received: 12 January 2010 / Accepted: 3 December 2010 / Published online: 15 January 2011

Abstract The problem of controlling a liquid drop suspended in an arbitrary two-dimensional elongational flow with vorticity is revisited. Bentley and Leal (J Fluid Mech 137:219–240, 1986) kept the drop centroid at the stagnation point using a linear proportional control strategy in a four-roll-mill apparatus that projects the drop's motion onto the stable flow direction of the stagnation point. A nonlinear strategy based on the Poincaré–Bendixson theory to ensure a periodic motion of the drop centroid inside a prescribed area around the stagnation point is proposed and studied. In addition, a detailed numerical study is presented to illustrate the effect of the control on the drop motion. The present strategy is effective, allowing for deformation and changes in the drop orientation by less than 1% for extreme flow conditions that cannot be achieved by a four-roll-mill setup.

Keywords Boundary-element method · Drop control · Elongational flows · Stokes flow · Two-roll mills

1 Introduction

The deformation of a liquid drop suspended in a flow is not yet fully understood for flows that induce large changes of the drop shape, for example, elongational flows. Large deformations can be produced by elongational flows whose rate of deformation is larger than the magnitude of the vorticity. Large deformations occur typically near stagnation points. However, a stagnation-point flow does not allow for long observation times due to the outgoing streamlines. A suitable control mechanism is essential to maintain the drop shape and position under known flow conditions for times that are long compared to the intrinsic time scales of the dynamics.

M. A. H. Reyes (✉)
Departamento de Termofluidos, Facultad de Ingeniería, Universidad Nacional Autónoma de México, Circuito Exterior, Cd. Universitaria, Coyoacán, 04510 Mexico, DF, Mexico
e-mail: mreyes@unam.mx

A. A. Minzoni
FENOMEC, Instituto de Investigaciones en Matemáticas Aplicadas y Sistemas, Universidad Nacional Autónoma de México, Apdo. Postal 20-726, Circuito Escolar, Cd. Universitaria, Coyoacán, 04510 Mexico, DF, Mexico

E. Geffroy
Instituto de Investigaciones en Materiales, Universidad Nacional Autónoma de México, Apdo. Postal 70-360, Circuito Exterior, Cd. Universitaria, Coyoacán, 04510 Mexico, DF, Mexico

Taylor [1,2] presented a four-roll mill apparatus (FRM) to study the large deformation of a drop in elongational flow, albeit only for short time intervals. Using a modern four-roll mill, Bentley and Leal [3] studied the drop dynamics at a stagnation point by implementing proportional control to ensure a fixed drop position for an extended period of time under known flow conditions. To control the drop position, a linear proportional mechanism was used that projects the motion of the drop along an incoming streamline, coinciding with the stable flow direction of the stagnation point. In this manner, the drift caused by the outgoing flow direction of the stagnation point is controlled. Among other important results, Bentley and Leal experimentally demonstrated the good performance of the control by adjusting the speed of all four rolls or cylinders. However, the effect of the control scheme on the drop parameters, including the Taylor deformation and the orientation angle, was not evaluated.

In this work, we revisit the problem of controlling a drop embedded in a two-dimensional elongational flow with significant vorticity from a numerical point of view. This flow is best produced with a two-roll mill (TRM) apparatus. A TRM can effectively generate flows where the ratio between the magnitudes of the rate of deformation and vorticity are greater than one [4,5]. This ratio is related to the dimensionless *flow-type parameter*

$$\alpha = \frac{\|\mathbf{D}\| - \left\|\overline{\mathbf{W}}\right\|}{\|\mathbf{D}\| + \left\|\overline{\mathbf{W}}\right\|}, \tag{1}$$

where $\mathbf{D} = \frac{1}{2}(\|\nabla\mathbf{u}\| + \|\nabla\mathbf{u}\|^T)$ is the rate-of-deformation tensor and $\overline{\mathbf{W}}$ is the *objective* vorticity tensor, which measures the rate of rotation of a particle with respect to the principal axes of $\mathbf{D}$ at that particle [6]. The case $\alpha = 0$ corresponds to simple shear flow, while $\alpha = 1$ describes a purely extensional flow. A vortex-dominated flow exists for $-1 \leq \alpha < 0$. For TRMs, the range of accessible values is $0 < \alpha \leq 0.3$ [7,8]. The FRM setup is most effective in the regime $0.4 \leq \alpha \leq 1$ [3,9]. With the TRM apparatus, a drop is placed near the stagnation point and is thus subjected to large deformation rates, as well as to rotation about its centroid. These conditions are difficult to achieve with the FRMs. A second significant flow parameter is the scalar shear rate, $\dot{\gamma} = \|\nabla\mathbf{u}\|$.

The implementation of the nonlinear control scheme in this work differs from that used by Bentley and Leal because it is based on the Poincaré–Bendixson principle for a planar system of two-dimensional ordinary differential equations describing the motion of a point particle (the centroid of the liquid drop) in a given velocity field. When a particle moves within a closed region containing a saddle point and the velocity field points inward at every point on the boundary, the particle undergoes a stable attractive periodic motion. Thus, given a prescribed tolerance region around the stagnation point, it is always possible to generate a controlled incoming flow whenever the center of mass of the liquid drop reaches the boundary of the tolerance region.

This perturbed flow is produced by adjusting the angular velocity of the cylinders, calculated using an analytical solution for the flow without significant change in the flow parameters, such as the shear rate and the flow-type parameter. This provides us with the time-dependent analogue of the Poincaré–Bendixson situation just described. The centroid of the liquid drop is locked into a perturbed attracting periodic trajectory around the saddle point, whilst it is confined to the prescribed tolerance area and to the prescribed values of all flow-field parameters. This mechanism is different from that of proportional control, which modifies the unstable nature of the saddle point by adjusting the angular velocities of the four cylinders to project the motion along the stable direction (incoming streamline) only. In the present control scheme, the effect of unstable directions combined with the flow readjustment produces a periodic motion of the centroid around the saddle point.

Given that no detailed studies of the influence of the control scheme on the deformation of a liquid drop are available, we study numerically the motion and deformation of a two-dimensional drop under the influence of the proposed control. The Stokes equations in a container are solved subject to the appropriate boundary conditions on the rolls and free surface of the drop. These equations are solved using the boundary-element method for a variety of flows and drop parameters. We study those perturbations introduced by the application of the control scheme and also provide the appropriate parameter values for future experimental studies.

In particular, an easily implemented control scheme is needed for experimental studies of the drop dynamics in elongational flows with vorticity and at small capillary numbers. These flows can induce large deformation of liquid drops and other objects such as capsules. Such studies provide insight into the breakup and coalescence of embedded objects. A possible application of TRMs with the control proposed in this work is the measurement

of the viscosity ratio or surface tension of fluid pairs by characterizing the evolution of the drop form, even for small drops with volume of a few picoliters. Experimental work is in progress to address these ideas. Other possible applications of this work concern emulsion technology and fluid transport in mature oil reservoirs.

The proposed technique is complementary to previous work [3,10], because it allows the detailed study of the long-time evolution of the liquid-drop parameters, mainly deformation and orientation. However, the possible flow regimes to be studied are not accessible to a FRM. The present work was carried out for several viscosity ratios and various geometric setups to assess the robustness of the proposed method and ensure a small influence it has on the liquid-drop behavior. The influence of the control scheme on the drop parameters is confirmed to be small (around 1%) with respect to the results for the nominal or idealized flow environment. The proposed control scheme is capable of redirecting the liquid-drop centroid toward the stagnation point on a time scale that is much shorter than that of the evolution, with minimal impact upon the liquid-drop dynamics for a wide range of viscosity ratios.

That is, Sect. 2 outlines relevant analytic results relating the rotational motion of the cylinders to the position of the stagnation point of the TRM flows of interest. In Sect. 3, the control problem is formulated and solved numerically. Section 4 presents results for a wide range of flow and geometric parameters. The last section is devoted to conclusions.

2 Approximate solution for flows generated by co-rotating two-roll mills

To assess the effect of the adjustment of rotation of the cylinders on the location of the stagnation point of the flow over a larger set of values of the parameters an analytical solution provides all possible behaviors. However, a solution that includes the effects of outside boundaries is not available. We thus resort to an approximation to the flow in the gap between the cylinders, which is obtained using a local solution approximately matched to the outer flow. We then tested the accuracy of this approximation by comparisons with the full numerical solution.

2.1 Local solution in bipolar coordinates

The convenient coordinate representation for a TRM device is the bipolar two-dimensional orthogonal curvilinear coordinate system, shown in Fig. 1, defined as [11, Sect. 2.9]

$$x = \frac{a \sin\eta}{\cosh\xi - \cos\eta}, \quad y = \frac{a \sinh\xi}{\cosh\xi - \cos\eta}, \tag{2}$$

or

$$\xi + i\eta = \log\left(\frac{x + \mathrm{i}(y+a)}{x + \mathrm{i}(y-a)}\right), \tag{3}$$

where $\xi \in (-\infty, \infty)$, $\eta \in [0, 2\pi)$.

The coordinate system has two foci at $(0, a)$ and $(0, -a)$. The curves of constant ξ are non-concentric circles given by

$$x^2 + (y - a\,\coth\xi)^2 = a^2\,\mathrm{csch}^2\,\xi$$

surrounding the positive focus for $\xi > 0$ and the negative focus for $\xi < 0$; e.g., describing the upper and lower cylinders in Fig. 1. Curves for constant η are circular arc segments of

$$(x - a\,\cot\eta)^2 + y^2 = a^2\,\mathrm{csc}^2\,\eta,$$

ending at the foci, when $x > 0$ for $0 < \eta < \pi$, and $x < 0$ for $\pi < \eta < 2\pi$.

The unit basis vectors, perpendicular and tangent to the cylinders surfaces, shown in Fig. 1, are, respectively,

$$\mathbf{e}_\xi = -\frac{\sinh\xi \sin\eta}{(\cosh\xi - \cos\eta)}\mathbf{i}_1 + \frac{(1 - \cosh\xi\cos\eta)}{(\cosh\xi - \cos\eta)}\mathbf{i}_2, \tag{4}$$

$$\mathbf{e}_\eta = \frac{(\cosh\xi\cos\eta - 1)}{(\cosh\xi - \cos\eta)}\mathbf{i}_1 - \frac{\sinh\xi\sin\eta}{(\cosh\xi - \cos\eta)}\mathbf{i}_2. \tag{5}$$

2.2 Approximate solution for the unbounded flow field

A co-rotating two-roll mill can effectively produce a two-dimensional flow with a stagnation point between the rolls or cylinders. Around the stagnation point, the flow is characterized by the *flow-type parameter*, α, and the shear rate, $\dot{\gamma}$. By varying the geometry of a TRM, the flow-type parameter is readily changed and experimental values from nearly 0 to 0.3 can be easily generated. For a FRM setup, the optimum parameter space has been shown experimentally to be in the range 0.4 to 1 [9]. Thus, TRMs are the *ad hoc* flow cell for studies of the dynamics of liquid drops in regimes complementary to FRM setups.

In this section, it is shown that for a given TRM geometry (see Fig. 1), the shear rate is a simple function of the angular velocity of the cylinders. The effect of the walls on the liquid drop can be systematically taken into account by adjusting the flow-cell geometry. The behavior of a liquid drop as a function of the capillary number and ratio of viscosities of the fluids can be studied by the appropriate choice of fluids.

Because our interest is in maintaining the position of the liquid-drop centroid close to the stagnation point, a simple description of the flow in this region is needed. In particular, a global description of the position of the stagnation point of the *unperturbed flow field* as a function of the geometry and the angular velocities of the cylinders is required. The unperturbed flow field is governed by the Stokes equation $\mu\nabla^2\mathbf{u} = -\nabla p$, and the continuity equation $\nabla \cdot \mathbf{u} = 0$, with boundary conditions $\mathbf{u}_i = \omega_i \times \mathbf{R}_i$ on the surface of the rolls and $\mathbf{u} = \mathbf{0}$ on the boundary of the container. We construct an approximate solution close to the stagnation point. To this end, consider the problem of two cylinders in an *infinite fluid* whose radii and angular velocities are R_1, ω_1 and R_2, ω_2. The surface of the cylinders is separated by a gap g. The apparatus is characterized by the geometric dimensionless parameter $r_g = g/\mathrm{de}$, where $\mathrm{de} = R_1 + R_2 + g$ is the separation between the axes of the cylinders.

The stream function of the flow field ψ satisfies the biharmonic equation $\nabla^4\psi = 0$. The stream function for an unbounded and co-rotating TRM in bipolar coordinates (ξ, η) (see Fig. 1), as in Jeffery [12], is

$$\begin{aligned}\frac{\psi}{h} &= A_0 \cosh\xi + B_0\,\xi\,(\cosh\xi - \cos\eta) + C_0 \sinh\xi \\ &\quad + D_0\,\xi\,\sinh\xi + K\,(\cosh\xi - \cos\eta)\log(\cosh\xi - \cos\eta) \\ &\quad + (A_1 \cosh 2\xi + B_1 + C_1 \sinh 2\xi)\cos\eta \\ &\quad + \sum_{n=2}^{\infty} (A_n \cosh(n+1)\xi + B_n \cosh(n-1)\xi \\ &\quad + C_n \sinh(n+1)\xi + D_n \sinh(n-1)\xi)\cos n\,\eta, \end{aligned} \tag{6}$$

where h is the metric factor

$$h = \frac{a}{\cosh\xi - \cos\eta}. \tag{7}$$

The logarithmic term is essential to account for the asymmetry of the flow [12]. The constant value of the coordinate ξ at the contour of the i-th cylinder is given by

$$\xi_{R_i} = \operatorname{arcsinh}\left(\pm\frac{a}{R_i}\right), \tag{8}$$

where

$$a = \frac{\sqrt{g\,(g+2R_1)\,(g+2R_2)\,(g+2R_1+2R_2)}}{2\,(g+R_1+R_2)}, \tag{9}$$

and the sign accounts for the position of the cylinders relative to the $\xi = 0$ axis.

The velocity field must satisfy the kinematic and no-slip boundary conditions at the surface of the cylinders. For the normal velocity component, the kinematic condition gives

$$u_\xi\left(\xi_{R_i}\right) = \frac{1}{h}\frac{\partial\psi}{\partial\eta}\bigg|_{\xi_{R_i}} = 0, \tag{10}$$

and the condition for the tangential velocity component requires

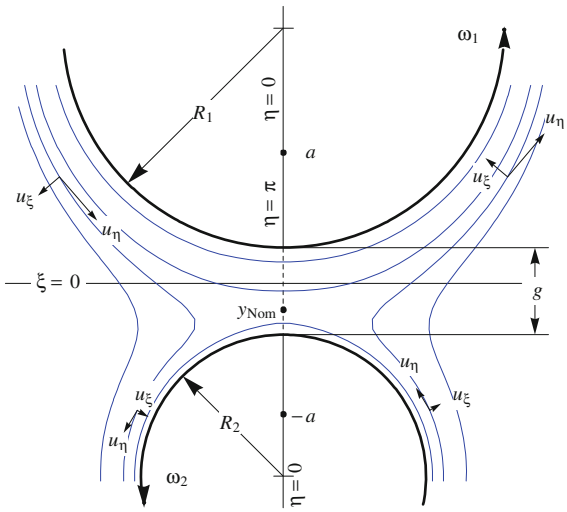

Fig. 1 Flow field generated by a corotating two-roll mill. Paths for several streamlines and the direction of the velocity's components at a few points are also shown. The position of the stagnation point y_{Nom} can be displaced along the dashed line by simply varying the ratio between the angular velocities ω_1/ω_2. For this geometry, this ratio is $\omega_1/\omega_2 = 0.549$, with $\alpha = 0.1156$, $R_1/R_2 = 1.549$, de $= 34$ and $r_g = 0.194$

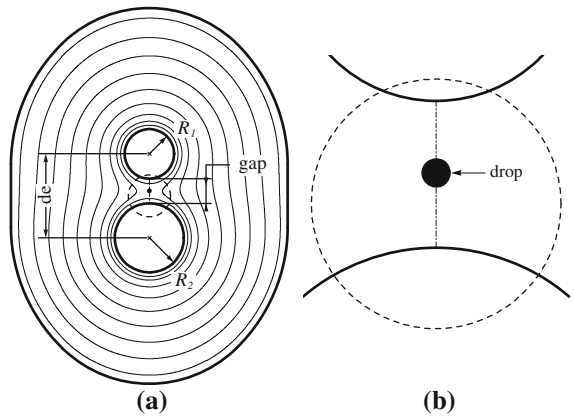

Fig. 2 The experimental TRM Cell **a** Streamlines for a TRM with an external boundary, the container, as calculated with the boundary-integral method. 128 elements are used for the cylinders and 500 elements are used for the container. The pair of cylinders have radii $R_1 = 10.00$ mm and $R_2 = 14.00$ mm; $de = 34.00$ mm. **b** Enlargement of the central region between the cylinders containing the stagnation point where the drop is positioned

$$u_\eta\left(\xi_{R_i}\right) = -\frac{1}{h}\frac{\partial\psi}{\partial\xi}\bigg|_{\xi_{R_i}} = -\omega_i\, R_i = \frac{a\,\omega_i}{\sinh\xi_{R_i}}. \tag{11}$$

The flow far from the cylinders must match the flow around the stagnation point shown in Fig. 2a. The numerical solution taking into account the boundary of the container, given in Sect. 3.2, shows that the flow away from the cylinders becomes horizontal along the $\eta = 0$ axis of symmetry. Thus, the vertical component of the velocity u_ξ tends to 0 at the line of symmetry $\eta = 0$, and away from the cylinders, as $\xi \to 0$. This gives

$$\lim_{\xi \longrightarrow 0,} u_\xi(\eta = 0) = A_0 + \sum_{n=1}^{\infty}(A_n + B_n) = 0. \tag{12}$$

To calculate the coefficients in (6), a Fourier series expansion in the η variable is carried out. Using [13, Eq. 1.514] the logarithmic term of the stream function (6) can be expressed as

$$\log(\cosh\xi - \cos\eta) \simeq \mathrm{a}_0 + \sum_{n=1}^{N}\mathrm{a}_n\cos n\eta, \tag{13}$$

where

$$\mathrm{a}_0 = \sqrt{\xi^2} - \log 2, \tag{14}$$

$$\mathrm{a}_n = -2\frac{\mathrm{e}^{-n\sqrt{\xi^2}}}{n}. \tag{15}$$

The product $(\cosh\xi - \cos\beta)\log(\cosh\xi - \cos\eta)$ is expanded as

$$(\cosh\xi - \cos\eta)\log(\cosh\xi - \cos\eta) \simeq \mathrm{b}_0 + \mathrm{b}_1\cos\eta + \sum_{n=2}^{N}\mathrm{b}_n\cos n\eta, \tag{16}$$

where

$$\mathrm{b}_0 = \mathrm{a}_0 \cosh\xi - \frac{\mathrm{a}_1}{2}, \tag{17}$$

$$\mathrm{b}_1 = \mathrm{a}_1 \cosh\xi - \mathrm{a}_0 - \frac{\mathrm{a}_2}{2}, \tag{18}$$

and

$$\mathrm{b}_n = \mathrm{a}_n \cosh\xi - \frac{\mathrm{a}_{n+1}}{2} - \frac{\mathrm{a}_{n-1}}{2}. \tag{19}$$

The Stokes solution, (6), is recast into the *approximate* form:

$$\begin{aligned}\frac{\psi}{h} \simeq\ & A_0 \cosh\xi + B_0\,\xi\,(\cosh\xi - \cos\eta) + C_0 \sinh\xi + D_0\,\xi\ \sinh\xi \\ & + K\left(\mathrm{b}_0 + \mathrm{b}_1\cos\eta + \sum_{n=2}^{N} \mathrm{b}_n \cos n\eta\right) + (A_1 \cosh 2\xi + B_1 + C_1 \sinh 2\xi)\cos\eta \\ & + \sum_{n=2}^{N} (A_n \cosh(n+1)\,\xi + B_n \cosh(n-1)\xi + C_n \sinh(n+1)\xi + D_n \sinh(n-1)\xi)\cos n\,\eta.\end{aligned} \tag{20}$$

Equation 10 of the kinematic boundary condition can be replaced by

$$\psi\left(\xi_{R_i},\ \eta\right) = M_{R_i}, \tag{21}$$

where ξ_{R_i} is the bipolar coordinate that represents the cylinder perimeter of radius R_i and M_{R_i} is the value of the stream function at the cylinder surface. Substituting this equation in (20) and arranging all terms proportional to $\cos n\eta$, an infinite system of equations is obtained for each cylinder,

$$\begin{aligned}& A_0 \cosh\xi_{R_i} + B_0\,\xi_{R_i} \cosh\xi_{R_i} + D_0\,\xi_{R_i} \sinh\xi_{R_i} \\ & + C_0 \sinh\xi_{R_i} + K\ \mathrm{b}_0\left(\xi_{R_i}\right) - \frac{M_{R_{1,2}}}{a}\cosh\xi_{R_i} = 0,\end{aligned} \tag{22}$$

$$-B_0\,\xi_{R_i} + A_1 \cosh 2\xi_{R_i} + B_1 + C_1 \sinh 2\xi_{R_i} + K\ \mathrm{b}_1\left(\xi_{R_i}\right) + \frac{M_{R_{1,2}}}{a} = 0, \tag{23}$$

and for $n \geq 2$

$$\begin{aligned}& A_n \cosh(n+1)\xi_{R_i} + B_n \cosh(n-1)\xi_{R_i} + C_n \sinh(n+1)\xi_{R_i} \\ & + D_n \sinh(n-1)\xi_{R_i} + K\ \mathrm{b}_n\left(\xi_{R_i}\right) = 0.\end{aligned} \tag{24}$$

Now substituting (20) in the boundary condition given by (11), the following expression is obtained

$$\begin{aligned}& -A_0 \sinh\xi_{R_i} - B_0\left(\xi_{R_i} \sinh\xi_{R_i} + \cosh\xi_{R_i}\right) - C_0 \cosh\xi_{R_i} - D_0\left(\xi_{R_i}\ \cosh\xi_{R_i} + \sinh\xi_{R_i}\right) \\ & + \left(B_0 - 2A_1 \sinh 2\xi_{R_i} - 2\,C_1 \cosh 2\xi_{R_i}\right)\cos\eta \\ & - K\ \sinh\alpha_R\left(1 + \mathrm{a}_0 + \sum_{n=1}^{N} \mathrm{a}_n \cos n\eta\right) + \frac{M_{R_i}}{a}\sinh\xi_{R_i} \\ & - \sum_{n=2}^{N} \cos n\eta\left((n+1)A_n \sinh(n+1)\xi_{R_i} + (n-1)B_n \sinh(n-1)\xi_{R_i}\right. \\ & \left. + (n+1)C_n \cosh(n+1)\xi_{R_i} + (n-1)D_n \cosh(n-1)\xi_{R_i}\right) \simeq \frac{a\ \omega_{R_i}}{\sinh\xi_{R_i}}.\end{aligned} \tag{25}$$

Collecting terms proportional to $\cos n\eta$, another Nth-order system of equations is obtained for each cylinder,

$$\begin{aligned}& A_0 \sinh\xi_{R_i} + B_0\left(\xi_{R_i} \sinh\xi_{R_i} + \cosh\xi_{R_i}\right) + C_0 \cosh\xi_{R_i} \\ & + D_0\left(\xi_{R_i} \cosh\xi_{R_i} + \sinh\xi_{R_i}\right) + K\ \sinh\xi_{R_i}\left(1 + \mathrm{a}_0\left(\xi_{R_i}\right)\right) - \frac{M_{R_i}}{a}\sinh\xi_{R_i} + \omega_{R_i}\left(\frac{a}{\sinh\xi_{R_i}}\right) = 0,\end{aligned} \tag{26}$$

$$-B_0 + 2A_1 \sinh 2\xi_{R_i} + 2\,C_1 \cosh 2\xi_{R_i} + K\ \mathrm{a}_1\left(\xi_{R_i}\right)\sinh\xi_{R_i} = 0. \tag{27}$$

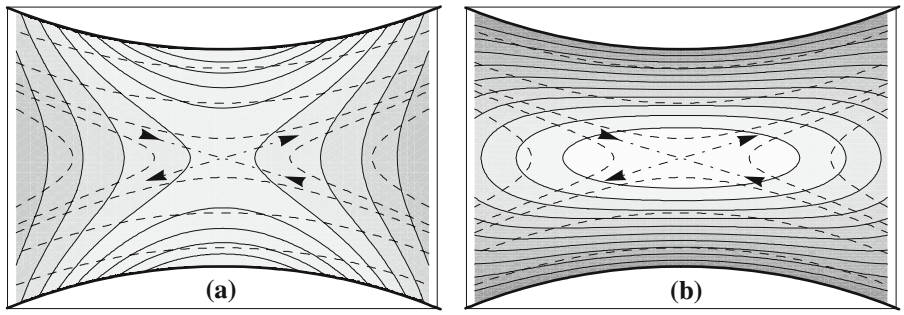

Fig. 3 Isopleths of **a** $\dot{\gamma}$ and **b** α in the gap region of a symmetric co-rotating TRM. *Dashed lines* are streamlines with *arrows* indicating the incoming and outgoing directions of the flow at the stagnation point. *Darker regions* correspond to lower values of the parameter. **a** The shear rate attains maximum values at the cylinder surfaces, whereas α is maximum within the central region about the stagnation point. This cell flow parameters are: $\omega_1 = \omega_2 = 0.2298$, $R_1 = R_2 = 14$, $g = 6$, $r_g = 3/17$, $\alpha = 0.1$

For $n \geq 2$,

$$(n+1)A_n \sinh(n+1)\xi_{R_i} + (n-1)B_n \sinh(n-1)\xi_{R_i} + (n+1)C_n \cosh(n+1)\xi_{R_i} + (n-1)D_n \cosh(n-1)\xi_{R_i} + K\ \mathrm{a}_n\left(\xi_{R_i}\right)\sinh\xi_{R_i} = 0. \tag{28}$$

For a given geometry, Eqs. 22, 23, 26, and 27 can be solved for the coefficients A_0, A_1, B_0, B_1, C_0, C_1, D_0 and M_{R_2} as functions of K, ω_1, and ω_2 for arbitrary values of M_{R_1}. Solving (24) and (28), the coefficients A_n, B_n, C_n and D_n are obtained as functions of K for each $n \geq 2$. For computational purposes, this infinite system was truncated at $N = 100$, providing a smoothly varying flow field for $N \geq 50$.

Finally, the coefficient K is obtained from (12) as a function of ω_1 and ω_2. Subsequently, for a given geometry, the coefficients of the stream function, velocity components, position of the stagnation point, and all other flow parameters are calculated as functions of the angular velocities ω_1 and ω_2.

2.3 Flow field in the experimental device

The control-scheme implementation on TRM apparatuses requires considering a bounded domain, as shown in Fig. 2. Thus, a numerical solution of Stokes flow was also computed using the boundary-integral method (see the following section) with its streamlines shown in Fig. 2a. This was obtained for a set of rollers of radii $R_1 = 10.00$ mm and $R_2 = 14.00$ mm and $de = 34.00$ mm. The perimeter form of the external container height is 152 mm with a width of 112 mm. These parameters were chosen to minimize the effect of the wall on the gap flow where the dynamics of a drop is studied, which is located around the stagnation point inside the gap between rollers, as shown in Fig. 2b. The shape of this perimeter corresponds to the mean streamline predicted by the approximate solution for a large set of roller radii.

To assess the validity of the approximate solution just obtained in the gap region around the stagnation point, a comparison was carried out between the numerical solution and the analytical solution for the flow in the absence of the liquid drop for the two relevant kinematic flow parameters: the shear rate $\dot{\gamma}$ and the *flow-type parameter* α. These parameters can be calculated at every point of the field as functions of both the TRM geometry and angular velocities. The comparison between the numerical solution and analytic approximation given in Sect. 2.2 was carried out for a wide variety of angular velocities and geometric parameters. The difference between the approximate and numerical solutions was in all cases less than 0.5% with respect to the numerical values. In Fig. 3, a typical flow in the gap region is shown, which is the most relevant domain for comparison between the analytical and numerical solutions. It must be noted that this flow does not take into account the presence of the liquid drop and is only valid in the low-Reynolds-number limit.

For a specific geometry, changes of the rotational speed of the cylinders produce a displacement of the stagnation point y_{ss} along the gap axis, as shown in Fig. 4, where the flow variables are given in terms of the dimensionless

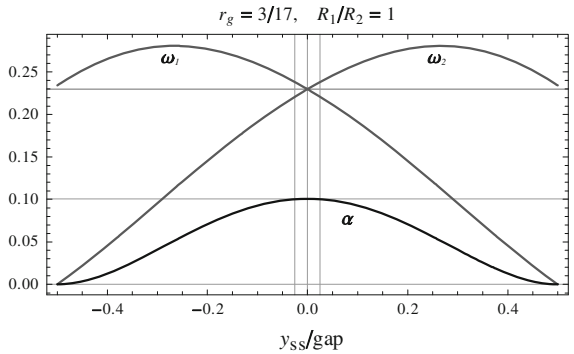

Fig. 4 Values of the flow-type parameter α and angular velocities ω_1 and ω_2 as functions of the position of the stagnation point across the gap for a symmetric geometry $R_1 = R_2, r_g = 3/17$ with constant value of the shear rate $\dot{\gamma} = 1$

gap, r_g. When $\dot{\gamma}$ is kept constant, the flow-type parameter becomes a slowly varying function of y_{ss}. Using these facts about the flow, we will show in the next section that the information displayed in Fig. 4 can be used to calculate the changes of the velocity of the cylinders needed by the control scheme.

3 Formulation and numerical solution of the control problem based on the Poincaré–Bendixson theory

In this section we use the central idea of the Poincaré–Bendixson theory (e.g. [14]) that produces a limiting periodic behavior around unstable points by balancing the outgoing flow at the stagnation point with a suitably chosen incoming flow.

3.1 Formulation of the control problem

Bentley and Leal [3] demonstrated that the only way to maintain the position of a liquid drop fixed with respect to the global flow field is by small local adjustments of the stagnation point position by tuning the angular velocities of the cylinders, with the constraint that these changes must not affect the flow-field parameters. A useful control scheme for TRMs or FRMs flows must maintain the liquid drop as close as possible to the stagnation point for a sufficiently long period of time compared with the time scale of the drop dynamics. From now on, the selected flow-field conditions of a TRM are called *nominal*. The properties of this nominal flow, such as the shear rate, flow-type parameter and the position of the stagnation point are denoted by the subscript Nom.

In order to describe the control scheme needed to maintain a liquid drop within the gap region of a TRM, as shown in Fig. 3, we consider a specific flow-field scenario. This is the case of a large liquid drop, say 1/5 of the gap size, whose center of mass is to be controlled inside a small tolerance area around the nominal stagnation point, typically of the order of 1/10 of the drop characteristic length (see the sketch in Fig. 5). This situation is appropriate for the study of the effect of nearby rigid boundaries on the drop dynamics or when meandering off the nominal stagnation point by the drop is not acceptable. The significance of understanding wall effects in elongational types of flow has not been addressed. The appropriate control scheme is presented here. In the results section, the effects of the flow-type parameter and viscosity ratios are detailed.

To construct the control scheme, the trajectory of the drop centroid is analyzed as the solution of a two-dimensional time-dependent dynamical system. We assume that the centroid is near the unstable saddle point, i.e., the stagnation point. If the vector field is incoming on the boundary of a box surrounding the unstable stagnation point, the system will settle into a periodic orbit inside the box, provided the vector field is time independent, as a consequence of the Poincaré–Bendixson theorem. When time dependence exists, a bounded motion, which can be periodic or quasi-periodic, is produced inside the box. This motion is equally as robust as in the time-independent case confining the liquid-drop centroid to any prescribed region, provided the appropriate incoming flow can be produced at the boundary.

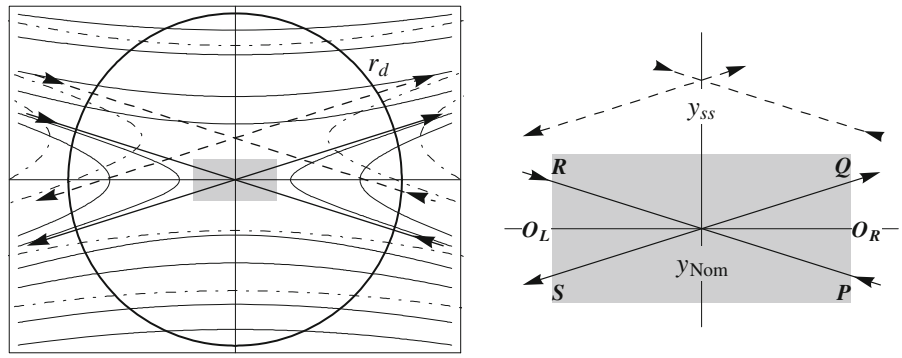

Fig. 5 The central region about the stagnation point shows a drop of radius r_d scaled with respect to a gap $g = 10\, r_d$. The control (tolerance) area is shown in grey with a length about $g/40$. **b** Blowup of the tolerance region. The nominal flow corresponds to the darker continuous lines, and the *dashed lines* show the relative displacement of the flow field during the controlled portion of the cycle

To define the control steps, we refer to Fig. 5b where the small tolerance area $PQRS$ is shown surrounding the nominal stagnation point. The flow field exits the tolerance region along the side $O_R Q$ and enters the side $O_L R$. The dark streamlines correspond to the nominal flow, while the dashed-dot flow lines correspond to the shifted stagnation point at y_{ss} resulting from the execution of the control scheme. Thus, during the controlled conditions, the velocity field is essentially reversed at sides $O_R Q$ and $O_L R$, while maintaining quasi-steady deformation stresses. That is, the drop centroid is advected towards the stagnation point at y_{ss} through the $O_R Q$ side, and exits via the $O_L R$ side. However, the rate-of-deformation tensor $\mathbf{D}$ and the objective vorticity tensor $\overline{\mathbf{W}}$ remain quasiconstant. Their length scales are larger than the characteristic length scale of the drop and the orientation and deformation of the liquid drop do not change significantly during the control step.

In Fig. 6 we display the centroid trajectory $ABCDEF$ of a full cycle of the control scheme. Let us assume that the centroid is initially at A at time $t = 0$, located inside the tolerance area shown in Fig. 6. In this position, the flow corresponds to the nominal conditions. The centroid is subsequently advected along the outgoing flow direction, reaching B at $t = t_{\text{on}}$ when the control step is initiated. The control mechanism displaces the stagnation point to y_{ss}, switching the flow field at B to a flow field leading the centroid towards the stagnation point y_{ss}. As a result, the centroid follows the flow lines along the path BC, arriving at C at time $t = t_{\text{off}}$. At t_{off}, the flow is reset to the nominal conditions and the stagnation point is moved back to the y_{Nom} position. Thus, the centroid is now advected towards the nominal stagnation point whilst being constrained into a loop about the stagnation point. For a centroid trajectory on the outside of the incoming axis, the full path corresponds to CD. At D the scheme is repeated, but now shifting the stagnation point to $-y_{ss}$ until the centroid reaches E where the stagnation point is shifted back to the nominal value and the centroid moves towards F where the process is repeated. The transit time spent along paths AB, CD and EF is much longer than the transit time along sections BC and DE because of the small eigenvalues associated with the corresponding incoming directions that produce the motion shown.

Note that the flow lines corresponding to $-y_{ss}$ behave in a symmetric manner relative to the symmetric tolerance area. A second centroid path for a full control cycle can be generated for a centroid starting at A, but incoming along the lines l_{in} in Fig. 6. In this trajectory the full cycle path can be constrained to one half the tolerance area. The angles θ_{Nom} and θ_{ss} are related to the flow-type parameter by

$$\theta = 2 \arctan\left(\sqrt{\alpha}\right), \tag{29}$$

where α takes the values α_{Nom} and α_{ss}, respectively, with $\alpha_{ss} \simeq \alpha_{\text{Nom}}$.

The purpose of the control scheme is to produce an incoming flow for the centroid of the drop *at the boundary of the tolerance area.* Thus, the center of mass is effectively moved as a dynamical system with an unstable fixed point (the stagnation point), but with a time dependent incoming field in an area surrounding the box. This arrangement guarantees the existence of a fixed periodic solution by the Poincaré–Bendixson theorem (see [14, Sect. 13.4]). Since

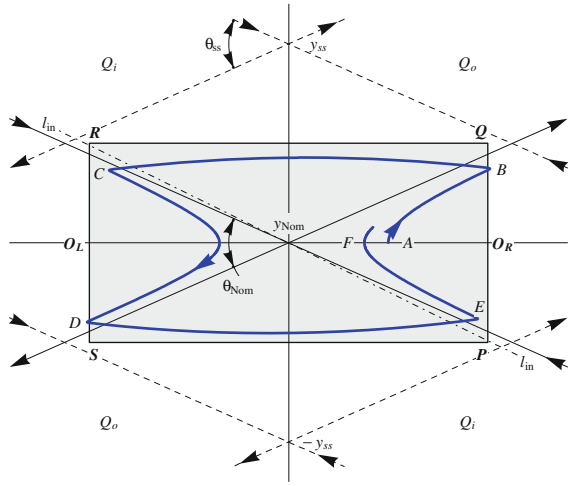

Fig. 6 Path $ABCDEF$ followed by the drop centroid subject to a control cycle. The centroid's trajectories during the controlled flow regime correspond to BC and DE, with the displaced stagnation-point position located at $\pm y_{ss}$, respectively. The angle between the incoming and outgoing streamlines at the nominal stagnation point θ_{Nom} and the angle at the corrective flow θ_{ss} have essentially the same values

the incoming vector field is time dependent, a bounded trajectory is obtained that is approximately periodic. This nonlinear procedure of balancing the repulsion at the critical point with the correction of the flow at the boundary of the tolerance region always produces a very robust bounded trajectory inside any prescribed area.

All displacements of the stagnation point are assumed to be carried out on a fast time scale compared with that of the drop dynamics. In the theoretical description given above, both the centroid of the drop and the streamlines are assumed to be known instantaneously. In a laboratory experiment, this will not be the case. The position of the centroid is determined after processing the flow field images and then the driving motors modify the flow field within a finite response time. These time lags must be taken into account in an experimental situation in order to calculate the effect of the control.

Three are the relevant times involved in an experiment: The time associated with the velocity of the video system in frames per second (fps) and the time of capture and processing of all images, τ_1. The finite response time, τ_2, of the cylinders to readjust their velocity as a consequence of the control, mainly due to the inertia of the mechanical system. And the response time, τ_3, of the fluid around the drop to the adjustment in the velocity of the TRM. The time τ_3 can be estimated as the diffusion time $\tau_3 = l^2/\nu$ based on the gap size g and the kinematic viscosity ν. The total response time, $\tau_1 + \tau_2 + \tau_3 = \tau_c$ must be smaller than the characteristic time τ_d of the internal motion of the drop, which is a function of the capillary number and viscosity ratio. For most up-to-date experimental environments, one can expect that $\tau_1 + \tau_2 \gg \tau_3$ given the material properties of the fluids and geometry of the setup, which corresponds to Stokes flow.

To determine the adjusted velocity field needed to ensure an incoming flow along $O_R Q$, i.e., after relocation of the stagnation point position to y_{ss} (or $O_L S$ for a displacement to $-y_{ss}$), a new flow line, assumed straight, is calculated entering the $O_R Q$ quadrant and exiting at y_{ss}; see Fig. 6. This requirement gives y_{ss} as a function of the size of the control area. Parametrizing the flow relationship as depicted in Fig. 4, the required rotational speed of the cylinder ω_1^c and ω_2^c can be determined as

$$\omega_i^c(t) = \omega_{\text{Nom},i} + \frac{\omega_i^c - \omega_{\text{Nom},i}}{2}\left(1 \pm \tanh\left(\frac{t - t_{\text{on}}}{\tau_c}\right)\right), \tag{30}$$

where t_{on} is the time when the centroid of the drop reaches the point B in a given cycle and ω_i^c and $\omega_{\text{Nom},i}$ correspond to the corrective and nominal rotational speed of cylinder i. The time scale τ_c accounts for the finite response time observed in an experimental environment. The positive sign applies when the control is near B and $t \simeq t_{\text{on}}$, at the imposition of the corrective flow step. At the end of the perturbed flow period, the control must return to the nominal flow conditions. Thus, the negative sign applies when the control reaches $t \simeq t_{\text{off}}$. The following step at point D is carried out in the same manner. It is remarked that, during the control steps, the flow parameter $\dot{\gamma}$ is kept constant, while the change in α is less than 0.5% for all cases.

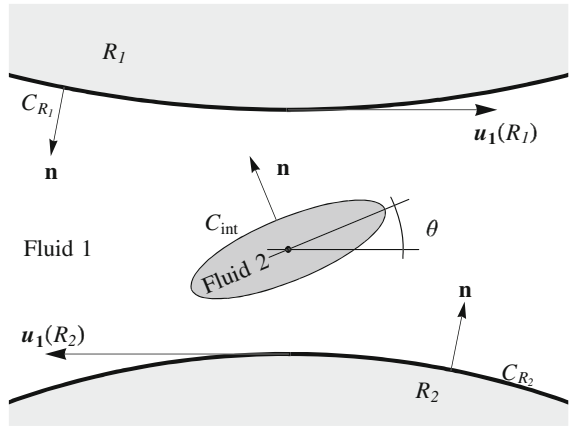

Fig. 7 Fluid interface deformed by a two-roll mill. θ is the orientation angle of the principal axis of the drop with respect to a horizontal line parallel to $\xi = 0$

This control is different from that used by Bentley and Leal [3]. The present control takes advantage of the knowledge of the local flow field and balances the unstable motion at the boundary of the tolerance region around the stagnation point with a time dependent incoming flow, giving an effective dynamical system with a periodic or quasi-periodic orbit for the centroid. In contrast, the control of Bentley and Leal modifies the flow, projecting the trajectory of the centroid along the stable direction at the nominal stagnation point. Essentially, the proportional method attempts to set the centroid of the drop back to the stagnation point. In this case, care must be taken to stabilize the control, as shown by Bentley and Leal. In the present situation, stability is achieved by the planar nature of the motion of the drop center of mass.

3.2 Numerical solution of the control problem

We now show numerically how the proposed control keeps the centroid of the drop within any prescribed tolerance area around the stagnation point of the nominal flow. Moreover, we show that the control mechanism changes the drop parameters by less than 1% from their nominal values.

The drop and suspending fluid are taken to be Newtonian and incompressible fluids with equal densities. Since only low Reynolds numbers are considered, the Stokes equations are appropriate, even if the angular velocities of the cylinders are time dependent. The geometry of the flow region is shown in Fig. 7, where the cylinders are only partially depicted and the container is not shown.

The suspending fluid is labeled as Fluid 1 with viscosity μ_1 and the drop is labeled as Fluid 2 with viscosity μ_2; $\lambda_\mu = \mu_2/\mu_1$ is the ratio of viscosities. The interface of the drop is denoted by C_{int}, the contours of the cylinders R_1 and R_2 are C_{R_1} and C_{R_2}, respectively, while C_c is the contour of the container and C_{rigid} is composed of the individual contours C_{R_1}, C_{R_2} and C_c. The boundary conditions are the no-slip conditions at the rigid boundaries given by the matching of the tangential velocity of the fluid to the velocity of the cylinders,

$$\mathbf{u}_1\left(C_{R_i}\right) = \boldsymbol{\omega}_{R_i} \times \mathbf{r}_{C_{R_i}}, \tag{31}$$

where $\mathbf{r}_{C_{R_i}}$ is the position vector for roller R_i with respect to the coordinates of the center of the cylinder. On the drop, the surface stresses at the interface are balanced by surface tension. The condition $\mathbf{u} = \mathbf{0}$ is imposed on the surface of the container. The stress jump across the interface is $\Delta\mathbf{f} = 2\kappa_m\sigma\mathbf{n}$, where κ_m is the mean curvature of the liquid drop and σ is the surface tension between the fluids.

The equations are formulated as boundary-integral equations for the velocity at the interface and the corresponding tractions at the boundaries. Following Pozrikidis [15] we use the two-dimensional Stokeslet Green function $\mathbf{G}$ to reduce the problem into solving an integral equation. This equation is found by multiplying the equations of motion by the Stokeslet $\mathbf{G}(\mathbf{x}, \mathbf{x}_0)$ and using the divergence theorem. This procedure gives two equations. One equation involves the unknown velocity on the interface of the drop, C_{int}, and the other equation involves the unknown stresses on the moving rigid boundaries, C_{rigid}:

$$-\frac{1}{4\,\pi\,\mu_1}\int\limits_{C_{\text{rigid}}}\mathbf{f}_{r,1}\,(\mathbf{x})\cdot\mathbf{G}\,(\mathbf{x},\mathbf{x}_0)\,\mathrm{d}l\,(\mathbf{x})+\frac{1-\lambda_\mu}{4\,\pi}\mathrm{PV}\int\limits_{C_{\text{int}}}\mathbf{u}_1\,(\mathbf{x})\cdot\mathbf{T}\,(\mathbf{x},\mathbf{x}_0)\cdot\mathbf{n}\,(\mathbf{x})\;\mathrm{d}l\,(\mathbf{x})-\frac{1+\lambda_\mu}{2}\mathbf{u}_1\,(\mathbf{x}_0)$$
$$=\frac{1}{4\,\pi\,\mu_1}\int\limits_{C_{\text{int}}}\Delta\mathbf{f}(\mathbf{x})\cdot\mathbf{G}\;(\mathbf{x},\mathbf{x}_0)\,\mathrm{d}l\,(\mathbf{x})-\frac{1}{4\,\pi}\int\limits_{C_{\text{rigid}}}\mathbf{u}_{r,1}\,(\mathbf{x})\cdot\mathbf{T}\,(\mathbf{x},\mathbf{x}_0)\cdot\mathbf{n}(\mathbf{x})\mathrm{d}l(\mathbf{x}),\tag{32}$$

when $\mathbf{x}_0$ is on C_{int}, and $\mathbf{T}(\mathbf{x},\mathbf{x}_0)$ is the Stresslet function. The same procedure on C_{rigid} gives:

$$-\frac{1}{4\,\pi\,\mu_1}\int\limits_{C_{\text{rigid}}}\mathbf{f}_{r,1}(\mathbf{x})\cdot\mathbf{G}\,(\mathbf{x},\mathbf{x}_0)\,\mathrm{d}l(\mathbf{x})+\frac{1-\lambda_\mu}{4\,\pi}\int\limits_{C_{\text{int}}}\mathbf{u}_1(\mathbf{x})\cdot\mathbf{T}\,(\mathbf{x},\mathbf{x}_0)\cdot\mathbf{n}(\mathbf{x})\,\mathrm{d}l(\mathbf{x})$$
$$=\frac{1}{2}\mathbf{u}_{r,1}\,(\mathbf{x}_0)-\frac{1}{4\,\pi}\mathrm{PV}\int\limits_{C_{\text{rigid}}}\mathbf{u}_{r,1}(\mathbf{x})\cdot\mathbf{T}\,(\mathbf{x},\mathbf{x}_0)\cdot\mathbf{n}(\mathbf{x})\mathrm{d}l(\mathbf{x})+\frac{1}{4\,\pi\,\mu_1}\int\limits_{C_{\text{int}}}\Delta\mathbf{f}(\mathbf{x})\cdot\mathbf{G}\;(\mathbf{x},\mathbf{x}_0)\,\mathrm{d}l(\mathbf{x}),\tag{33}$$

when $\mathbf{x}_0$ is on C_{rigid}.

The normal vector $\mathbf{n}$ is directed away from the rigid boundaries and from the fluid interface into the suspending fluid. In Eq. 33, $\mathbf{f}_{r,1}$ is the unknown traction at the rigid boundaries on the suspending fluid; see [15, Eqs. 2.6.17 and 2.6.20]. The velocity $\mathbf{u}_1$ is the unknown velocity of the suspending fluid at the fluid interface. The velocity $\mathbf{u}_{r,1}$ is the known velocity of the suspending fluid at the rigid boundaries. Finally, $\Delta\mathbf{f}$ is the stress jump at the fluid interface which is known in terms of the curvature of C_{int}. The notation PV indicates the Cauchy principal value of the integral, and the tensors $\mathbf{G}$ and $\mathbf{T}$ are the two-dimensional free space Stokeslet and Stresslet, respectively [15].

The kinematic conditions at the free surface require that the drop surface is advected with the flow. This gives

$$\frac{\partial\mathbf{x}}{\partial t}(s,t)=[\mathbf{u}_1(s,t)\cdot\mathbf{n}]\,\mathbf{n},\tag{34}$$

where s is a Lagrangian marker variable used to identify the interfacial points, $\mathbf{u}_1$ is the velocity of the fluid over the interface, and $\mathbf{n}$ is the normal vector directed from the fluid interface to the suspending fluid.

The linear equations for $\mathbf{u}_1$ and $\mathbf{f}_{r,1}$ are solved, once the curve C_{int} is known. Then, the kinematic equation (34) for the curve is solved to advect C_{int}, using a second order Runge–Kutta scheme. To preserve the accuracy of the scheme, the radial position, with respect to the centroid, of the Lagrangian markers is rescaled after an appropriate number of steps, to conserve the volume of the drop. Also, the Lagrangian markers are distributed along the interface. This gives the required conservation of area implied by the equation of motion. The proper scaling factor is the ratio between the area of the drop at the current time to the initial area.

In order to couple the evolution equation (34), with the control equation (30), we need to calculate the centroid of the drop as a function of time to determine the switching times where the centroid reaches the edge of the tolerance region. Denoting by $\bar{x}$ and $\bar{y}$ the x- and y-positions of the centroid, we have

$$\bar{x}=\frac{\frac{1}{2}\int_{C_{\text{int}}}x^2\,\mathrm{d}y}{A},\quad\text{and}\quad\bar{y}=\frac{\int_{C_{\text{int}}}x\,y\,\mathrm{d}y}{A},\tag{35}$$

where A is the area of the liquid drop. The functions x and y are the interpolating functions representing the interface in terms of the arc length s along the surface. The integrals (35) are calculated analytically in their interpolation representation and provide a fast feedback in the control setup.

4 Results

We describe results on the performance of the proposed control in maintaining the centroid of a two-dimensional drop inside the tolerance region in a flow field generated by a symmetric co-rotating two-roll mill. The control performance was studied by comparing the numerical solution for a drop with its centroid fixed at the nominal stagnation point—the reference values, as well as the polar trajectories, are labeled with the subscript R_f—against the numerical solution of a controlled drop whose centroid is initially displaced from the nominal stagnation point.

Table 1 Geometries of the symmetric co-rotating TRMs used in the numerical tests, $r_g = g/\mathrm{de}$ is the geometric ratio, α is the value of the flow-type parameter at y_{Nom}, ω_{Nom} is the angular velocity for the nominal flow field, ω_+ and ω_- are the angular velocities required to carry the stagnation point at the position $\pm y_{ss}$

TRM	r_g	α_{Nom}	ω_{Nom}	ω_+	ω_-	$\Delta\alpha$ (%)
A	0.41176	0.3027	0.84633	0.88408	0.80816	−0.37
B	0.30294	0.1988	0.49605	0.51605	0.47530	−0.44
C	0.17647	0.1007	0.22982	0.23815	0.22090	−0.50

The angular velocities are calculated for a constant value of the shear rate $\dot{\gamma} = 1$

The data for reference conditions were obtained by readjusting the center of mass of the drop at the stagnation point after each time step.

The liquid-drop parameters compared are the Taylor deformation parameter D_T and the drop orientation measured by the angle θ between the major axis of the drop and the horizontal $\xi = 0$ axis. The deformation is given by

$$D_T = \frac{L - B}{L + B}, \tag{36}$$

where L and B are the long and short axes of an ellipsoidal drop shape. Variations in the deformation ΔD and orientation $\Delta\theta$ are calculated as $\Delta D = \left(D_T - D_{Rf}\right)/D_{Rf}$ and $\Delta\theta = \left(\theta - \theta_{Rf}\right)/\theta_{Rf}$, respectively.

The control scheme was tested with three symmetric TRM geometries corresponding to values of the flow-type parameter at the nominal stagnation point of $\alpha \approx 0.1, 0.2$ and 0.3, and for drops of several viscosity ratios, $\lambda_\mu = 0.1, 0.5, 1.0, 5.0, 10.0$ and 20.0. In all cases, the shear rate was kept as $\dot{\gamma} = 1.0$ in both the nominal flow field conditions and the corrective flow field. The initial shape of the drop is circular and the ratio between its diameter and the gap was fixed to $r_d = 0.2g$ in order to introduce some effects due to the presence of rigid boundaries near the drop. The surface tension σ is adjusted to give the capillary number $\mathrm{Ca} = r_d\,\dot{\gamma}\,\mu_1/\sigma = 0.3$. For the viscosity ratios and the flow-type parameters studied, the behavior of the drop in the nominal flow-field conditions shows critical values of the capillary number corresponding to both drops that evolve to a stationary shape (subcritical) and drops that eventually break-up (supercritical) [10].

The control parameters were chosen as follows. For the tolerance area, the horizontal distance X_{Tol} was taken as 2.5% the gap size and the vertical distance Y_{Tol} was half the gap size. The angular velocities of the rollers for the corrective flow field correspond to those for which the stagnation point is displaced 2.5% of the gap size in both directions. This value ensures that the incoming and outgoing flow lines at the stagnation point at the position y_{ss} are above the tolerance area, as shown in Fig. 6. In all tests, the initial (unstable) position of the centroid of the drop was $(X_{\mathrm{Tol}}/4, 0)$.

Table 1 contains information about the TRM geometries selected, the values of the flow-type parameter, and the angular velocities of the nominal flow condition. The corrective flow is induced by angular velocities ω_i^c for the cylinders given by ω_+ and ω_- for $y_{ss} \geq 0$. Then $\omega_1^c = \omega_-$. The column to the right shows the difference in the value of α due to the angular velocity variation.

The effect on the drop dynamics due to changes in the flow field imposed by the control scheme is measured by comparing the behavior between a drop subjected to a controlled flow field to that of a drop whose centroid is positioned exactly at the stagnation point and is subjected to nominal flow field conditions (the reference condition).

Figures 8, 9 and 10 are polar plots of the evolution of the Taylor deformation D_T and orientation angle θ for several viscosity ratios following the ideas of Torza et al. [16] and Rallison [17]. Figure 8 corresponds to the geometry $A(\alpha = 0.3)$, Fig. 9 to $B(\alpha = 0.2)$ and Fig. 10 to $C(\alpha = 0.1)$. The duration of these simulations was $120\dot{\gamma}$, except for the case of $\lambda_\mu = 5.0$ of the geometry A, for which $t = 70\dot{\gamma}$. For Fig. 8, the form parameters of drops with viscosity ratios higher than $\lambda_\mu \geq 5$ correspond to non-stationary shapes. On the other hand, the drop forms for all viscosity ratios to attain stationary values for $\alpha < 0.3$.

The curves of the drop form shown in Figs. 8, 9 and 10 all take into account the control scheme with no differences observed with respect to the deformed shapes of those drops fixed at the stagnation point. The long-term

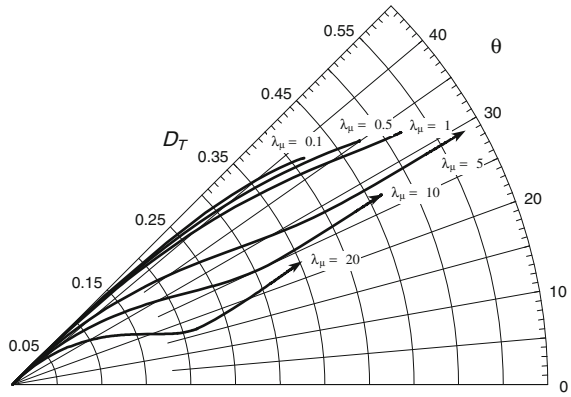

Fig. 8 Polar plot of the deformation parameters versus orientation for drops with Ca $= 0.3$ for the TRM A geometry ($\alpha = 0.3$). The curves corresponding to the viscosity ratios $\lambda_\mu = 0.1$, 0.5 and 1.0 arrive to a stationary state, whereas the curve for $\lambda_\mu = 5.0$, $\lambda_\mu = 10.0$ and 20.0 (ending in an arrow) do not attain an stationary shape at the end of the simulation; for these cases the drop will deform until break-up. All the simulations have a total time $T = 120\dot{\gamma}$ except the simulation that corresponds to $\lambda_\mu = 5.0$ where the time is $T = 70\dot{\gamma}$

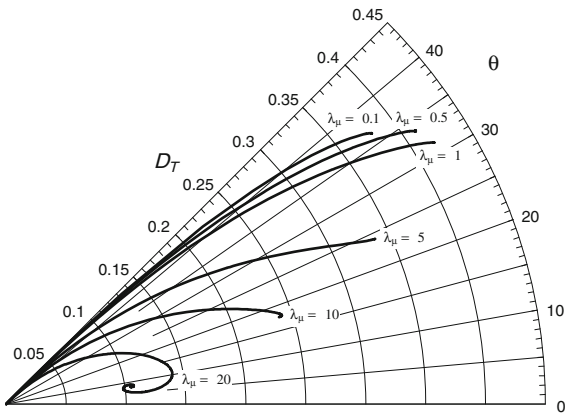

Fig. 9 Polar plot of the deformation parameter versus orientation for drops with Ca $= 0.3$ for the TRM B geometry ($\alpha = 0.2$). All the curves arrive to a stationary state

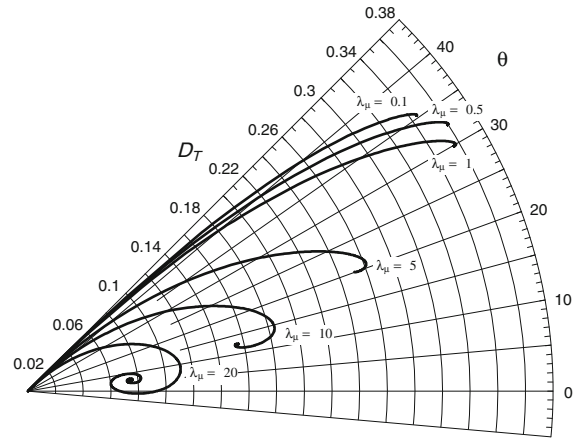

Fig. 10 Polar plot of the deformation parameter versus orientation for drops with Ca $= 0.3$ for the TRM C geometry ($\alpha = 0.1$). All curves arrive to stationary states. However, trajectories for high viscosity values—$\lambda_\mu \gtrapprox 20$—may have section with negative orientation angles

orientation of low-viscosity drops ($\lambda_\mu < 1$) is not influenced significantly by the flow-type parameter, maintaining an orientation of 45° with respect of the flow axis; i.e., orientation values close to the principal eigenvalue of the deformation tensor as can be seen in Figs. 8 and 9. However, with higher α values, drops attain a more elongated form—$D_T \simeq 0.5$—due to a weaker rotational motion.

For higher-viscosity drops, the influence of the flow parameter on orientation is more distinctive, with drops aligning more strongly with the flow ($\theta \to 0$ as $\alpha \to 0$; see Fig. 7). In addition, once a drop aligns with the flow away from the principal eigenvalue, the maximum deformation attained diminishes. In these cases, a higher viscosity reduces the inner flow and induces a weak deformation with a strong rotation. The drop quickly settles into a small deformation with a fast and persistent spinning mode. Experiments in progress show this latter drop behavior.

These results qualitatively match the theoretical prediction by Rallison [17] for small deformations $O(\mathrm{Ca}^2)$, the experimental results of Torza et al. [16] for simple shear flows, and those of Bentley and Leal [10] under elongational flows with a proportional control scheme.

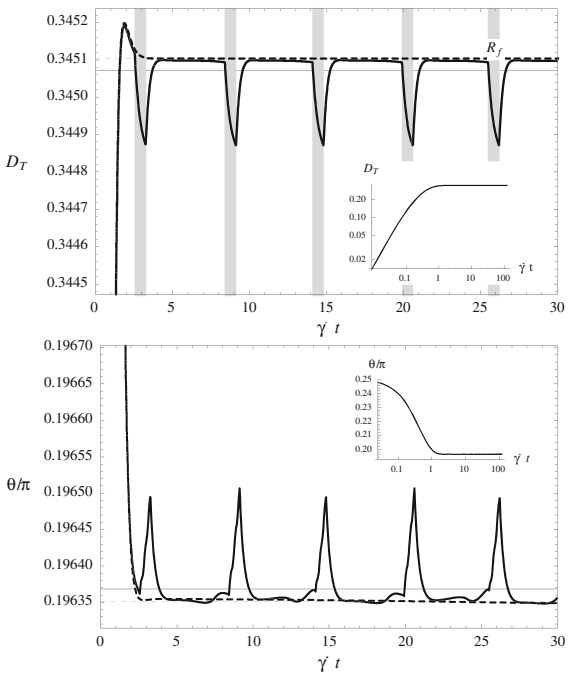

Fig. 11 High-resolution plots of the deformation (*top graph*) and orientation of a drop (*bottom*) in the TRM-*C* geometry ($\alpha = 0.1$) with $\lambda_\mu = 0.1$. The *dashed traces* are the reference case (the drop fixed at the stagnation point). The continuous curve is the controlled case. Oscillations of form are due to effects of the corrective flow field. *Insets* present the complete time evolution of deformation and orientation monotonically attaining steady-state values

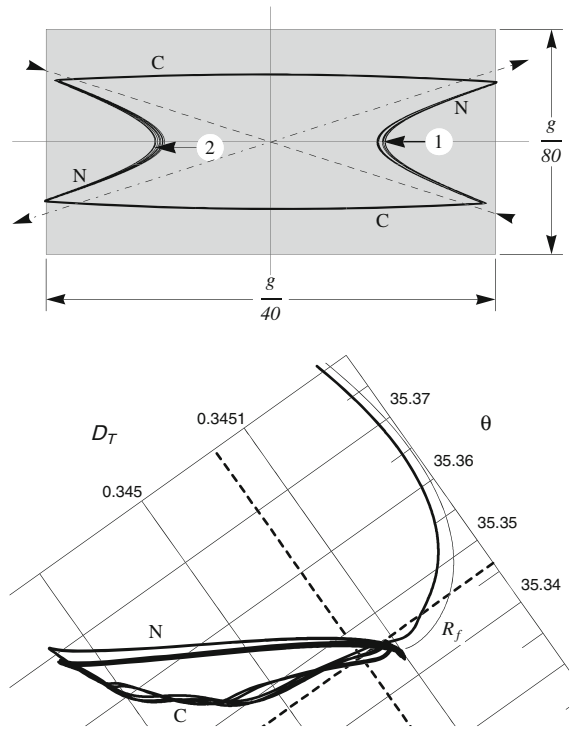

Fig. 12 Trajectories of the drop centroid in the TRM-*C* geometry for $\lambda_\mu = 0.1$. The *N* labels indicate trajectories under nominal flow conditions, *C* labels are the trajectory under the corrective flow produced by the control. Bullet 1 indicates the initial position of the centroid of the drop and Bullet 2 indicates the final position after $120\dot{\gamma}$. The thick trace on the polar plot shows the periodic motion around the mean stationary values, the latter shown as a pair of crossed *dashed line*. The R_f trace, starting at the top, corresponds to the late form evolution for a drop fixed at the stagnation point

Figures 11, 12, 13, 14, 15 and 16 describe numerical simulations for viscosity ratios $\lambda_\mu = 0.1$, 10.0 and 50 for every pair of figures, subjected to the weakest elongational flow: $\alpha = 0.1$. These results show the effects of the control scheme on the evolution of deformation and orientation values of a drop as well as on the centroid trajectory and the detailed polar plots of the periodic behavior of the drop form after long times. The small insert shows the time evolution of these form parameters, with the full plots showing their corresponding high resolution time dependent values. For the high resolution plots in Figs. 11, 13 and 15, the top graphs correspond to evolution of the deformation and the bottom graphs to the corresponding evolution of the orientation. The horizontal lines on the deformation and orientation plots represent their asymptotic values at long times. In both graphs, the broken lines give the result for the fixed stagnation point, at nominal flow conditions, while the full line are the result of the controlled process. The grey bars show the time interval of adjustment of the speeds of the rolls.

In Figs. 11 and 12, a low viscosity scenario is presented with $\lambda_\mu = 0.1$. Figure 11 shows a drop that evolves in time monotonically towards the steady shape; see insert of top and bottom graphs. However, the detailed evolution shows a weak periodic trace in synchrony with the controlled flow, with average values close to the nominal values during a time interval less than 25% of the time evolution. The adverse effects on the maximum variation of relative deformation are less than 1%, and those of the relative orientation are even weaker, oscillating within a few arc-minutes. Figure 12 shows the path of the drop centroid about the nominal stagnation point (top graph) as well as details of the drop shape at long times via a high resolution polar plot (bottom graph) about the steady state

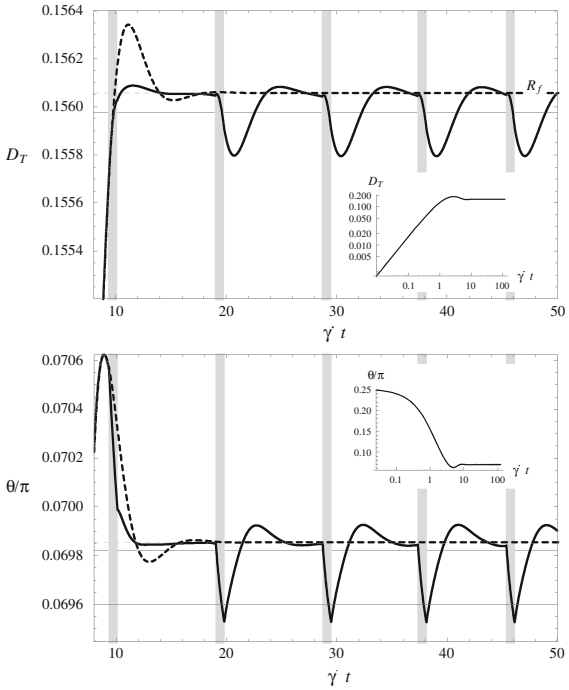

Fig. 13 High-resolution plots of deformation (*top*) and orientation (*bottom*) of a drop for $\lambda_\mu = 10.0$ and $\alpha = 0.1$. *Dashed lines* are the reference case; *continuous curve* are the controlled case. The unwanted oscillatory effects are due to the corrective flow field. *Insets* are the complete time-evolution traces

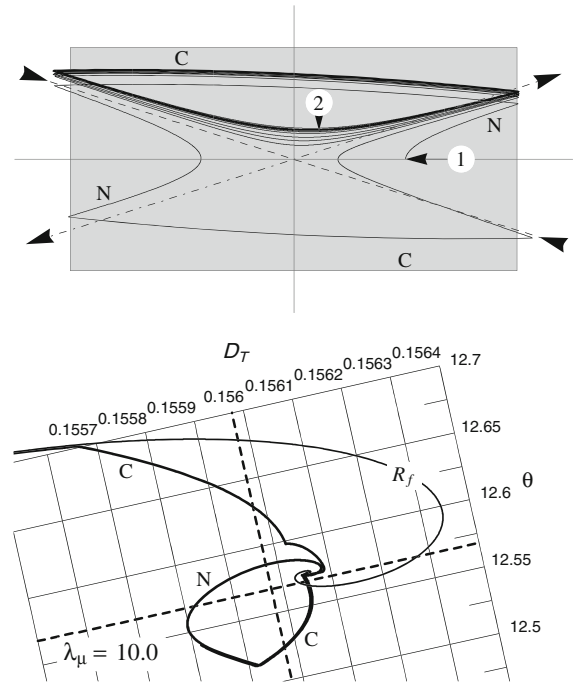

Fig. 14 Trajectories of the drop centroid for $\lambda_\mu = 10.0$ and $\alpha = 0.1$. *N* and *C* labels, and bullets 1 and 2 indicate same events as Fig. 12. The high-resolution polar plot shows both the R_f with overshoots on the deformation and orientation, as well as the periodic motion around the mean stationary value, with the *dashed lines* locating the mean-drop-form values. The upper *C* curve section correspond to the corrected centroid trajectory induced by $-y_{ss}$

form values. The deformation trajectory for the drop fixed at the stagnation point is depicted by the R_f trace. The drop oscillatory motion reduces its deformation and increases its orientation slightly. The drop centroid trajectory remains within the tolerance region and attains a form with variations that are small and practically periodic.

In Figs. 13 and 14, a similar simulation is presented, but for a drop with a viscosity ratio of $\lambda_\mu = 10$. The variation of the drop parameters as a result of the control scheme is small, with a small orientation oscillation at short times and a similar oscillation in Taylor's deformation; see both inserts in Fig. 13. This behavior is similar to that observed experimentally in concentrated polymer solutions by Geffroy and Leal [7] and theoretically by Singh and Leal [18] under similar flow fields. In this case, however, surface tension may induce the over- and under-shoot elastic behaviors. Upon the imposition of the controlled flow, overshoots are observed for Taylor's deformation and the orientation angle. It appears that the characteristic time of the drop is longer than the time under modified flow conditions. In the top graph of Fig. 14, we note that a time lag in the control scheme generates an overshoot of the centroid's trajectory beyond the upper left side of the tolerance area and a bias towards the upper portion of the tolerance region.

Figures 15 and 16 show results for a drop with a viscosity ratio of $\lambda_\mu = 50$ and a long-lived transient behavior is seen. In particular, Fig. 15 shows a characteristic time for the drop shape dynamics significantly longer than the time for modified flow conditions, which is longer than several cycles of the control scheme. These figures again show a small and persistent influence of the control upon the deformation and orientation. However, these alterations have relative values of less than 1% for low viscosities, while ΔD_T attains values close to $\pm 12\%$ for the drop with $\lambda_\mu = 50$ for $t = 70\dot{\gamma}$. The orientation angle can vary by as much as $\Delta\theta = \pm 3^\circ$. The latter behavior for the drop form persists for the duration of the simulation.

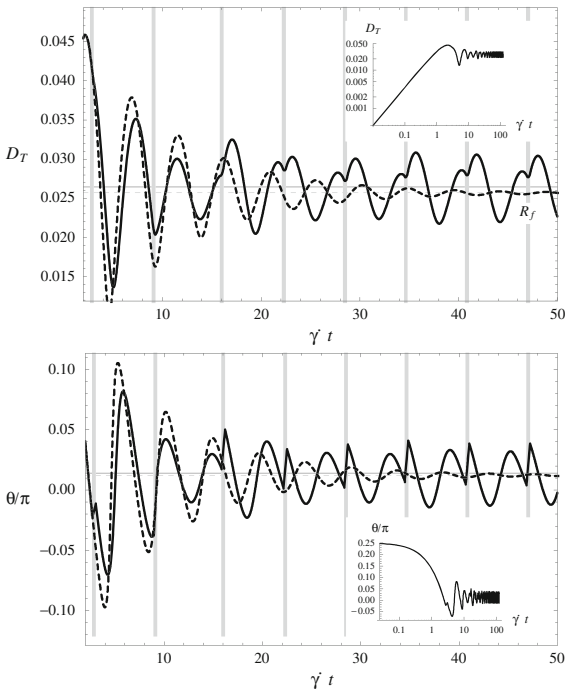

Fig. 15 Deformation and orientation of a drop with $\lambda_\mu = 50$ and $\alpha = 0.1$. *Insets* show the time dependence of these parameters with corresponding high resolution graphs. The predicted long time weak oscillations are unwanted effects due solely to the corrective flow field

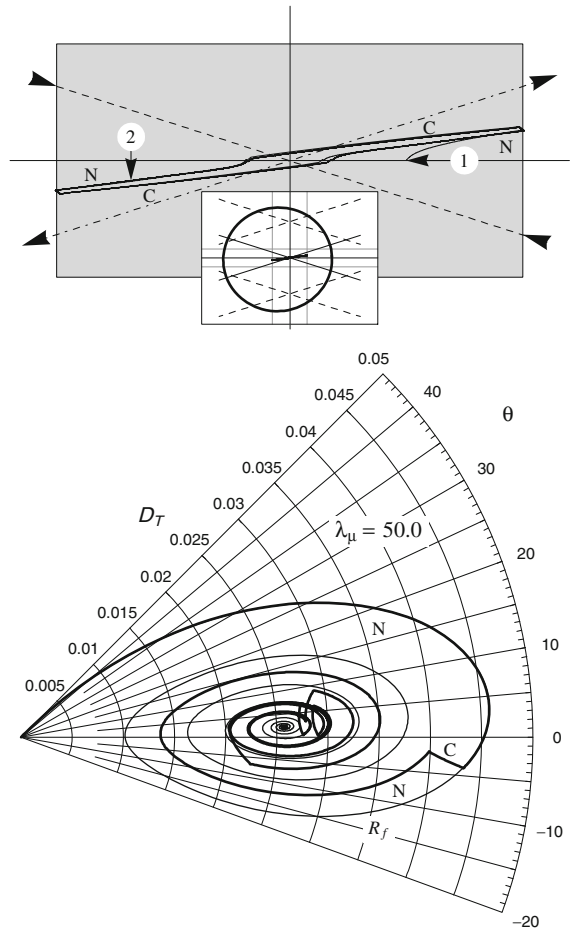

Fig. 16 Trajectories of the drop centroid for $\lambda_\mu = 50.0$ and $\alpha = 0.1$ (*top graph*). *N* and *C* indicate nominal and corrective flow conditions. Bullet 1: initial position; Bullet 2 final position of the centroid after 120 $\dot{\gamma}$. The *insert* on the centroids trajectory shows the size of the control domain relative to the drop size. The polar curve (*bottom*) shows a long periodic path for the drop form around the mean stationary values for the reference and the controlled-drop scenarios

In the insert of Fig. 16, we show a circular drop, and the incoming and outgoing flow lines at the nominal stagnation point. The short line around the stagnation point corresponds to the trajectory of the drop centroid generated during the control process. The locations of the control stagnation points are depicted by the broken lines. The actual magnified drop trajectory is shown in the full figure.

The shape evolution of a high-viscosity drop, shown in the polar plot at the bottom of Fig. 16, presents a slowly decaying oscillation, achieving small deformations coupled with positive and negative orientation angles, overshooting past the x-axis. For the total simulation time shown, the persistent oscillation does not reach long-term quasi-stationary values. In this plot, the dark line shows the control phase, which does not change the oscillatory motion; but only avoids as described the outflow drift. Whenever the drop orientation is decreasing and the control flow is imposed simultaneously, this coupling of form and flow dynamics appears as the source of the long-lived transient of the drop form seen in the simulation. Thus, a weak inner flow and weak stress differences due to surface

tension facilitate a drop to spin during many cycles. The latter behavior is independent of the control scheme, as shown by the reference trajectory R_f. This figure shows the good performance of the proposed control, with a clear decoupling of drop and control time scales for a large range of viscosity ratios.

A simple variation of the proposed control can be implemented for cases where the drop trajectory overshoots past the tolerance domain, as shown in Fig. 14. In this case, the incoming axis can be modified, correcting the angle θ_{Nom} by a factor $m > 1$ and moving the incoming flow line to the position shown by l_{in} in Fig. 6. In this case, the drop will be capable of reaching and entering the incoming flow axis very accurately. The optimal value of m can depend on the delay time τ_c, and should be determined experimentally in each case. For all the theoretical cases analyzed in this work this parameter was set to 1.0.

5 Conclusions

We have shown that a simple approximate solution for the flow generated by a TRM setup provides the basic ingredient for constructing a stable and robust strategy for controlling the liquid drop position under extreme flow conditions not accessible to FRM flows. A solution relating the local flow geometry to the control parameters explicitly was used to construct the incoming flow at the boundary of the tolerance region. This produces the bounded motion of the centroid since the unstable motion induced by the outflow at the stagnation point is balanced by the incoming nature of the controlled flow at the boundary of the tolerance region as required by the Poincaré–Bendixson theory.

The proposed scheme can control the centroid of a drop within a prescribed region. It was found that a tune-up of the incoming streamlines can provide a long residence time for the drop under nominal flow conditions, which is a desirable feature in experimental studies.

For all cases analyzed, the results were obtained under the assumption of a two-dimensional two-phase flow. This assumption is most likely valid for a large class of regimes in experimental conditions, particularly those studied here; i.e., for small Ca numbers and small values for Taylor's D_T. This is because values for the three-dimensional components of the surface-tension forces are not very different from those for the two-dimensional case, see, e.g. [19,20]. On the other hand, three-dimensional effects will be most relevant for drops with unbounded D_T under high viscosities and high α values, such as those shown in Fig. 8. Under this latter scenario, these simulations may not provide accurate quantitative comparisons with experimental data, such as the critical deformation or flow strain for drop break up, nor predicted values for the shape evolution of the drop, among others. However, preliminary experiments in progress indicate that the control performs its task for real drops, even for very high viscosity ratios.

The numerical results show that the present control has a small influence on the evolution of the drop, less than 5% for a wide range of flows and fluid viscosities. This quantification is not available from previous studies.

The present ideas can be used to control other immersed objects, such as capsules, cells, etc. (see [21]), provided that one knows the unperturbed flow in a simple enough way to rapidly compute the feedback loop, appropriate for the object to be controlled.

Acknowledgments MAHR thanks DGAPA-UNAM PROFIP Program for support for his stay at IIMAS-UNAM. AAM thanks the FENOMEC program. EG thanks CONACyT for the research grants by CONACyT. We also want to sincerely thank the anonymous reviewers for their careful review of the first version of this work, whose comments led to a much improved version, and the Associate Editor, Prof. Pozrikidis, for helpful suggestions on the presentation.

References

1. Taylor GI (1932) The viscosity of a fluid containing small drops of another fluid. Proc R Soc Lond A 138:41–48
2. Taylor GI (1934) The formation of emulsions in definable fields of flow. Proc R Soc Lond A 146:501–523
3. Bentley BJ, Leal LG (1986) A computer-controlled four-roll mill for investigations of particle and drop dynamics in two-dimensional linear shear flows. J Fluid Mech 167:219–240
4. Reyes MAH, Geffroy E (2000) Study of low Reynolds number hydrodynamics generated by symmetric co-rotating two-roll mills. Revista Mexicana de Física 46(2):135–147

5. Reyes MAH, Geffroy E (2000) A co-rotating two-roll mill for studies of two-dimensional, elongational flows with vorticity. Phys Fluids 12(10):2372–2376
6. Astarita G (1979) Objective and generally applicable criteria for flow classification. J Nonnewton Fluid Mech 6:69–76
7. Geffroy E, Leal LG (1992) Flow birefringence of a concentrated polystyrene solution in a two roll-mill 1. Steady flow and start-up of steady flow. J Polym Sci B Polym Phys 30(12):1329–1349
8. Wang JJ, Yavich D, Leal LG (1994) Time resolved velocity gradient and optical anisotropy in lineal flow by photon correlation spectroscopy. Phys Fluids 6(11):3519–3534
9. Yang H, Park CC, Hu YT, Leal LG (2001) The coalescence of two equal-sized drops in a two dimensional linear flow. Phys Fluids 13(5):1087–1106
10. Bentley BJ, Leal LG (1986) An experimental investigation of drop deformation and breakup in steady two-dimensional linear flows. J Fluid Mech 167:241–283
11. Arfken G (1971) Mathematical methods for physicists, 2nd edn. Academic Press, New York
12. Jeffery GB (1922) The rotation of two circular cylinders in a viscous fluid. Proc R Soc A 101:169–174
13. Gradshteyn IS, Ryzhik IM (1981) Tables of integrals, series and products. Academic Press, New York
14. Ross S (1984) Differential equations. Wiley, New York
15. Pozrikidis C (1992) Boundary integral and singularity methods for linearized viscous flow. Cambridge University Press, Cambridge
16. Torza S, Cox RG, Mason SG (1972) Particle motions in shear suspensions. J Colloid Interface Sci 38(2):395–411
17. Rallison JM (1980) A note of the time-dependent deformation of a viscous drop which is almost spherical. J Fluid Mech 98(3): 625–633
18. Singh P, Leal SG (1994) Computational studies of the FENE dumbbell model in a co-rotating two-roll mill. J Rheol 38:485–517
19. Acrivos A (1983) The breakup of small drops and bubbles in shear flows. Ann N Y Acad Sci 404:1–11
20. Stone HA (1994) Dynamics of drop deformation and breakup in viscous fluids. Annu Rev Fluid Mech 26:65–102
21. Pozrikidis C (2003) Modeling and simulation of capsules and biological cells. CRC Press, London